Incremental solidification (toward 3D-printing) of magnetically-confined metal-powder by localized microwave heating

Mihael Fugenfirov, Yehuda Meir, Amir Shelef, Yuri Nerovny,
Eli Aharoni and Eli Jerby
Tel Aviv University, Tel Aviv, Israel

Abstract

Purpose – This paper aims to present an experimental and theoretical study oriented to investigate the potential use of localized microwave-heating (LMH) in 3D-printing and additive-manufacturing (AM) processes.

Design/methodology/approach – Following a previous study by the authors, a magnetic confinement technique is developed here as a non-contact support for the incremental solidification by LMH of small metal-powder batches. This approach, which saves the need for a mechanic support in contact with the powder-batch during the microwave heating, may significantly simplify the LMH–AM process.

Findings – The powder properties are characterized, and a theoretical LMH model is used to simulate the LMH mechanism dominated here by magnetic eddy currents.

Originality/value – The experimental products are analyzed, and their hardness, porosity and oxidation are evaluated. Practical considerations and further improvements of the non-contact LMH–AM process are discussed.

Keywords Additive manufacturing, 3D printing, Sintering, Localized microwave heating

Paper type Research paper

1. Introduction

Besides mass production in manufacturing industries, there is a growing demand for custom-made products designed for specific needs (hence, manufactured in small quantities or even single units). Additive manufacturing (AM) and 3D-printing techniques enable efficient production of such specifically tailored designs, and may save time and raw materials (Conne *et al.*, 2014). Moreover, AM is capable of manufacturing complicated designs, sometimes difficult or even impossible to realize by conventional techniques, such as casting or machining.

While various plastic-based AM systems have become popular in the last decade (Levy *et al.*, 2003) (even as small 3D printers for domestic usage), metal processing is still the industrial sector with the higher-priced components. Lasers are widely used for AM of metal parts in various schemes. In the selective laser sintering (SLS), the object is produced layer-by-layer from a powder bed, heated locally by a scanning laser beam (Frazier, 2014; Santos *et al.*, 2006; Li *et al.*, 2010).

Microwaves are mainly known as useful for volumetric solidification and sintering of metal powders (Roy *et al.*, 1999), as well as for processing of metal-based materials and metal casting (Mishra and Sharma, 2016). The localized microwave heating (LMH) effect, such as applied for microwave drilling (Jerby *et al.*, 2002), can also be used for AM (Jerby *et al.*, 2015) by partial melting and solidification of small batches of metal powders in incremental steps. As proposed in Jerby *et al.* (2015), microwave devices could be simpler and smaller than lasers, but their resolution is essentially poorer. Hence, LMH-based AM systems might be more suitable for relatively rough construction processes. Their main advantages in such large-volume operations, with respect to existing high-resolution laser-based AM systems, might be their potentially lower cost, higher efficiency (in terms of electric power and raw material usage) and faster throughput.

The concept of contact-less magnetic fixation of the metal-powder batch, preliminarily introduced in Jerby *et al.* (2015), may significantly advance the LMH–AM applicability; hence, it is further investigated in this study. The attractive force induced in the metal powder is demonstrated, numerically and experimentally, as an effective means to confine the powder batch in a contact-less manner during its microwave heating. A theoretical model is used to characterize the powder's properties and to evaluate the LMH mechanism, dominated here by the microwaves' magnetic-field component and the powder's complex permeability. The experiments presented are intended to produce metal rods in order to investigate elementary construction operations by LMH–AM. The properties of the experimental products are examined, and their quality is evaluated.

2. Methods

Unlike typical laser-based AM processes, using layer-by-layer techniques, the LMH–AM process (Jerby *et al.*, 2015) uses small batches of metal powder as additive elements (namely, *voxels*). The metal powder is fed in a form of compacted batches into the interaction region. The localized microwave irradiation melts each voxel, which is consequently solidified as a *bead* and incrementally merged with the previously constructed structure. The experimental LMH–AM process is illustrated in Figures 1(a) and (b).

In our previous study (Jerby *et al.*, 2015), each batch of metal powder was encapsulated in a small ceramic or glass tube, as a mechanical holder that supports the powder-batch in a confined manner during its microwave heating process. This arrangement was instrumental for the principle feasibility demonstration of the LMH–AM concept, but it may impose significant difficulties in practice due to the presence of the supporting tube in contact with the molten powder during the entire process.

2.1 Magnetic confinement of the metal-powder batch

Here, we use an external static magnetic field as a means to hold the metal powder-batch in a confined form, with no physical contact. Each powder batch is initially packed in a cylindrical feeder, as illustrated in Figure 1(a). This support is removed once the powder is magnetized and stands still (before the LMH), as illustrated in Figure 1(b). This contact-less technique, preliminarily presented in Jerby *et al.* (2015), saves the need for ceramic or glass supports in contact with the molten powder during the microwave operation.

The force $\mathbf{F_M}$ applied on the powder particles by the static magnetic flux density $\mathbf{B}$ is given by Griffiths (2007) as:

$$\mathbf{F_M} = \nabla(\mathbf{m} \cdot \mathbf{B}) \tag{1}$$
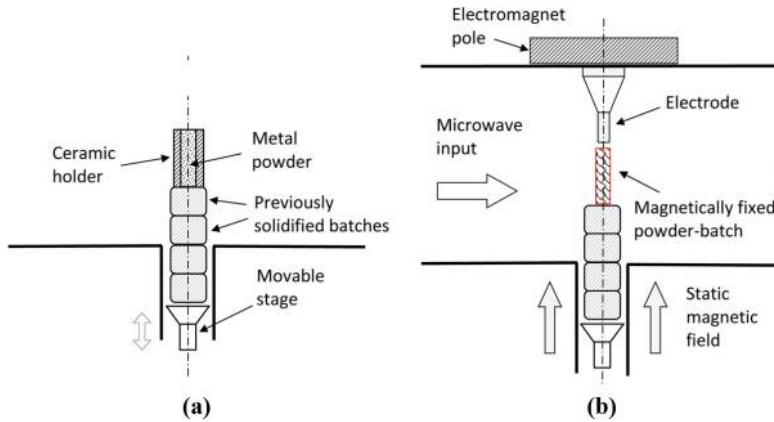
Notes: The localized microwave power is applied in a stepwise manner to
successive batches of metal powder, which are solidified and incrementally form
a structure (a metal rod in this case). (a) At each step, the packed metal powder
batch is positioned first on top of previously solidified structure by a mechanical
means, followed by the application of a static magnetic field to keep the
confined powder batch standstill while removing the mechanical support; (b) the
microwave radiation is locally applied then to the exposed powder batch to and
melt it

Figure 1.
Conceptual
illustrations of the
experimental
LMH–AM process

where **m** is the magnetic moment of the particle, given by $\mathbf{m} = m_p\boldsymbol{\sigma_M}$ and m_p is the
particle mass and $\boldsymbol{\sigma_M}$ is the induced magnetic moment per mass. The inter-particle
interaction exerts a force between each two adjacent particles, which is attractive for in
line and repulsive for parallel orientations, as illustrated in Cases (1) and (2), respectively,
in Figure 2(a) [given the angle β between the magnetic dipole vector and the orientation
vector connecting the two particles' centers, the force is attractive for $|\beta| < 55°$ and
repulsive for $|\beta| > 55°$ (Lumay *et al.*, 2009)]. Other forces enhancing the powder fixation
are caused by gravitation, friction, moisture and capillary effects (Herminghaus, 2005).
However, the magnetic attraction between the particles (e.g. Wang *et al.*, 2013) is
considered to be the dominant force.

To verify the dominance of the attracting forces in the magnetically confined metallic
powder, as observed in Jerby *et al.* (2015), a magnetostatics model was simulated using
CST Studio Suite® software (Ver. 2016). In the model geometry displayed in Figure 2(b),
the bunch of particles is simulated as a cubic structure of $5 \times 5 \times 5$ spheres. The static
electric and magnetic properties assigned for these metal particles are $\sigma = 7 \cdot 10^6$ S/m,
$\mu_r = 1000$ and $\varepsilon_r = 1$, where σ is the electric conductivity, and μ_r and ε_r are the relative
magnetic permeability and dielectric permittivity, respectively (the subscripts r and 0
denote relative and vacuum values, respectively). The spherical particles of $20\text{-}\mu$m
diameter each are assumed to be perfectly arranged in the cubic structure, except one
particle, which deviates from the outer face of the cube to a distance up to 10 μm. The
simulation results confirm the attracting force exerted on this particle by all the other, as
shown in Figure 2(c), for various values of the static magnetic field applied to confine the
powder. This attracting force tends to minimize the total magnetic energy W_M, which is
given by:

Figure 2.
Mutual forces exerted among metal particles under static magnetic fields
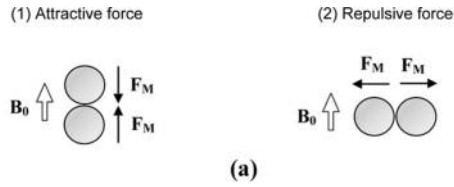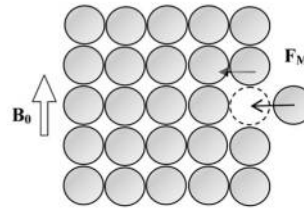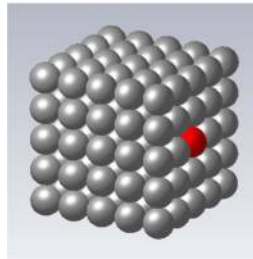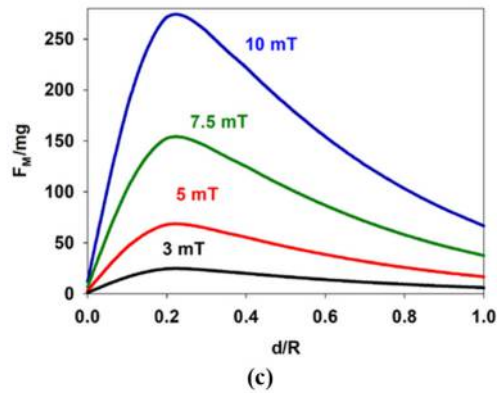
Notes: (a) Two particles generate attractive and repulsive forces where situated in in-line (1) and parallel (2) orientations, respectively; (b) a model of 125 particles is under a static magnetic field in a cubic arrangement, whereas one particle (marked Red) is deviating from the cubic structure and hence subjected to an attractive force; (c) graphical representation showing the simulation results of this force with respect to the distance of deviation d (normalized to gravitation mg and particle radius R, respectively) for various values of the externally applied static magnetic-field

$$W_M = \frac{1}{2}\int_V \mathbf{B} \cdot \mathbf{H}\, dV \qquad (2)$$

where V is the entire volume shown in Figure 2(b) (left) and $\mathbf{H} = \mathbf{B}/\mu$ is the static magnetic field strength. The minimal value of the total magnetic energy is attained indeed by a perfectly packed cube of metal particles. Yet, the intensity of the magnetic field applied here (<10 mT) is not sufficient to initially organize the particles, but only to keep them confined (once arranged by another means).

2.2 Experimental setup
A block diagram of the experimental setup is depicted in Figures 3(a) and (b). The LMH effect is enhanced in the microwave cavity by an electrode [shown in Figure 3(b)], which concentrates the electric field into the powder-batch region, and initiates therein a thermal-runaway instability (Jerby *et al.*, 2005). The electrode is made of a 2.4-mm$^{\varnothing}$ tungsten rod, and the cavity cross-section is 100×50 mm^2. The LMH interaction is conducted in air atmosphere during these experiments.

The iron-based powder used in the LMH–AM experiments presented here is the commercial DirectSteel-20 powder (EOS GmbH) designed for laser sintering. Its elemental
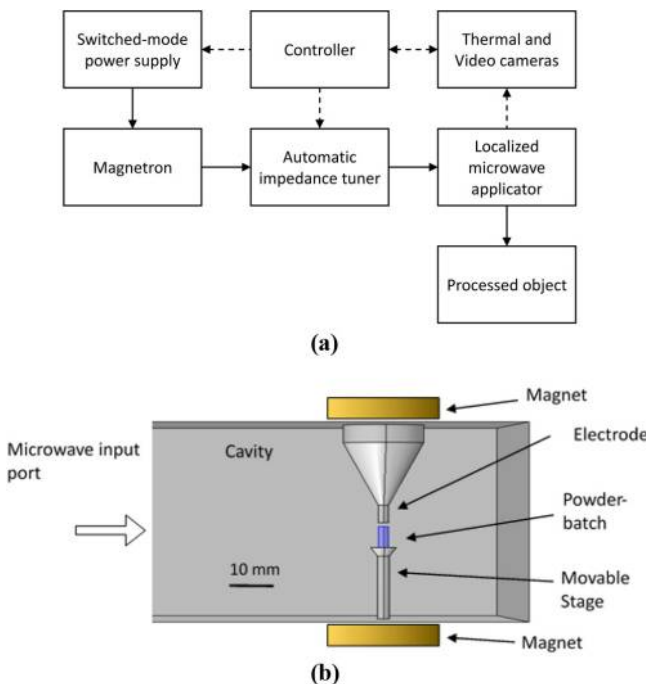
Notes: (a) A block diagram; (b) the LMH interaction region.
The powder-batch is placed in the microwave cavity on a movable
stage, which enables the extension of the solidified region

Figure 3.
The LMH–AM
experimental setup

composition, analyzed by SEM back-scattered electrons (BSE) and energy-dispersive X-ray spectroscopy (EDS), includes iron, nickel and copper (in approximately 70, 23 and 7 per cent atomic ratio, respectively).

The volume of the powder batch added in each run is approximately 15 mm^3. The powder batch is inserted into a cylindrical support and mechanically compacted, and then subjected to a static magnetic field. The latter keeps the batch confined in a cylindrical shape (as in Figure 4), and hence, the mechanical support can be removed before the LMH begins. A magnetic field of approximately 3 mT is sufficient for the non-contact fixation of the metal powder.

The experimental setup uses a 2.45-GHz, 1-kW magnetron powered by a switched-mode converter (MagDrive-1000, Dipolar, Sweden). The microwave reflections are analyzed and minimized by an adaptive auto-tuner (Homer, S-Team, Slovakia). A thermal camera (A305SC, FLIR, Sweden) in the range of 470-1,400K and a video camera are used for diagnostic purposes. A LabView code controls the experiment and accumulates the measured data for later analyses.

After the magnetic fixation of the powder batch, a microwave pulse of approximately 0.8 kW peak is applied in each step for a period of approximately 3 s. The electrode initiates the LMH process by concentrating the microwaves into the powder batch. The incident and reflected microwave-power components are detected by the Homer auto-tuner, and recorded by the LabView code.

After the microwave power is turned off, the molten batch is cooled down and solidified. Its outer surface is cleaned from soot by a metal brush; the next batch of powder is placed on top of it, and the process repeats as shown in Figure 4.

The feasibility of incremental solidification of metal powders under a static magnetic field by LMH is studied in various aspects, aimed at the successive stages of the AM
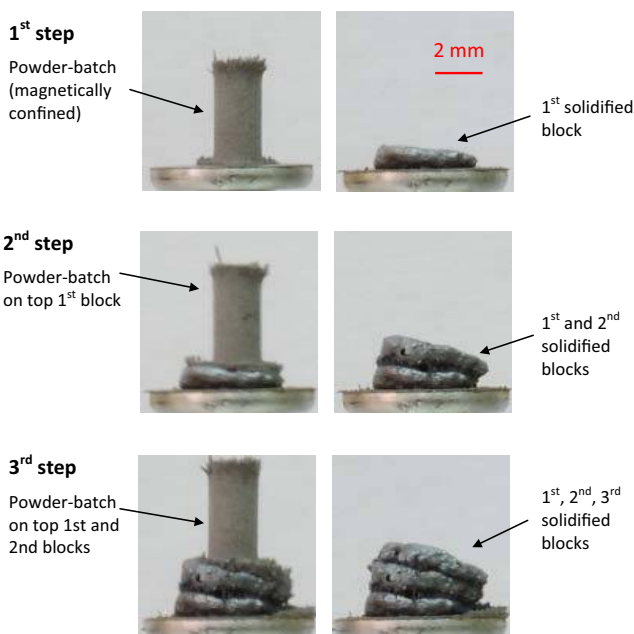

Figure 4.
The contact-less magnetic confinement of powder-batches and their LMH incremental solidification process shown, for example, in three successive steps

process. The first stage is intended to examine the LMH of the powder batch and its solidification to form the basic additive element. The second stage is directed to the solidification and merging of additional powder batches, on top of the previously solidified structure. The final stage is aimed at the further extension of the constructed object by repeating the steps of powder solidification and consolidation.

3. Experimental results

Facing the challenge of constructing complicated structures by LMH–AM, we first examined the process by making single rods in an incremental manner. Using the contact-less magnetic fixation technique in the experimental setup shown in Figures 3(a) and (b), our main objectives here are to validate and to further improve the preliminary results presented in Jerby *et al*. (2015).

The intense LMH interaction also generates a plasma plume ejected from the powder during ∼0.15 s at the beginning of the process, as shown in Figure 5(a), (b) and (c). As found here, the plasma absorbs a significant part of the microwave power. After the microwave pulse, the molten powder is solidified in a nearly ellipsoidal shape of ∼3-4 mm diameter and ∼1-2 mm height, which forms the elementary solid product of this LMH–AM process. In the next step, as shown in Figure 4, the movable base is lowered by 1-2 mm to retain the same geometrical conditions. Another batch of powder is placed on top of the previously solidified structure, and the LMH process is repeated again under the same conditions. Consequently, the next powder batch is solidified and consolidated with the previous structure underneath. An example for the first three steps of the LMH–AM process is presented in Figure 4.

The absorbed microwave power and the measured temperature rise in a single batch are presented in Figure 6. The corresponding incident power shows that the delivered and absorbed energies are approximately 0.2 kJ/mm^3 and 0.17 kJ/mm^3, respectively. The

(a)   **(b)**   **(c)**
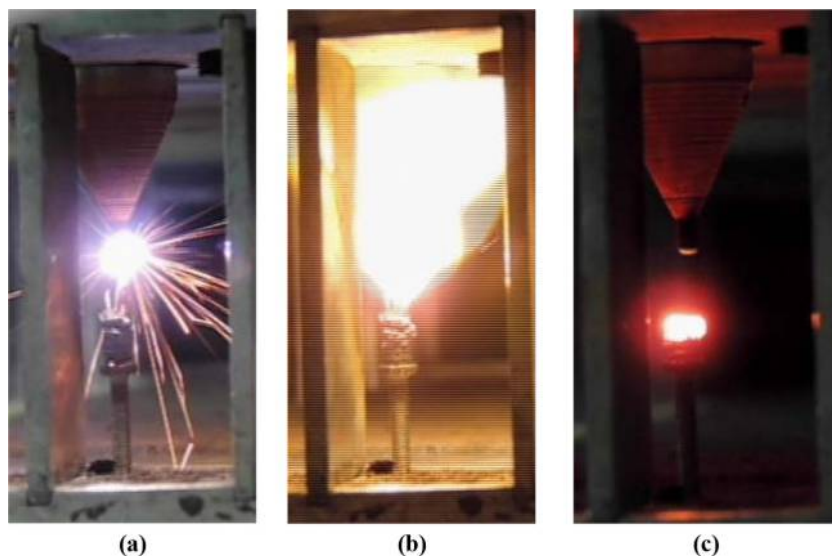
Notes: (a) Heating; (b) plasma emission; (c) the molten powder batch is solidified after the microwave power is turned off

COMPEL

temperature increases up to approximately 1,100 K in approximately 2.5 s, which implies having a relatively short heating transient in comparison with the observed larger time constant of the Newton's Law of cooling (in the order of approximately 70 K/s) for the molten powder after the microwave irradiation has been turned off [it is noted though that (a) the temperature measurements, taken above 500 K, are subjected to some uncertainties due to the rapid heating rate, the small voxel size and the plasma ejection; and (b) the iron powder emissivity is >0.85 at the measured temperature, which is higher than the solid iron due to the air holes (Sih and Barlow, 2004), and the emissivity variation in this range is limited to <5 per cent].

Figure 7 shows the stepwise LMH–AM process. In each step, the powder is placed and solidified in a nearly similar form, on top of the previous block. A approximately 13-mm long solid rod, created in 11 repetitive steps, is shown in Figure 8(a). The corner shape presented in Figure 8(b) consists of two such rods brazed by LMH of another powder batch in between them. This result also demonstrates the ability of joining two solid parts using LMH.

The mechanical properties of the LMH–AM products were tested as follows:

- Density measurements using Archimedes' law showed an average density of approximately 4.2 g/cm^3 (compared to approximately 6.3 and 7.1 g/cm^3 obtained by laser and conventional sintering, respectively).

- Optical microscope observations of the products' cross-sections revealed pores in both the bulk and interface regions. The relative porous volume coincides with the density results.

- Micro-structure analyses by SEM–BSE of the product's internal structure revealed various domains of solidified metal, metal-oxide and pores, as shown, for example, in Figure 9.

- Micro-hardness measurements of the LMH–AM products, performed by a Vickers indenter for 15 s with 0.5 and 1 Kg loads, resulted in 152 ± 24 and 158 ± 15 HV, respectively, on average. The indentations were measured at the product cross section in the bulk, in both the metal and metal-oxide regions, as seen in the inset in Figure 9. It is noted that the hardness specified for laser sintering is 225 HV, in a proportion similar to the density ratio of the products obtained.
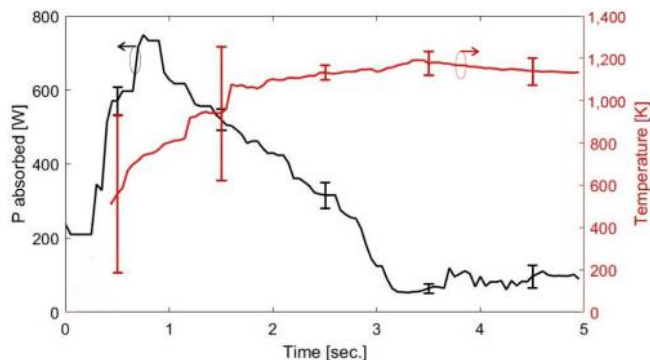

Figure 6.
Measurement results of the absorbed microwave power and of the temperature evolved on the powder-batch surface above 470 K

Note: Average results accumulated in ten experimental runs with typical spreads represented by the error bars

Step No.	Powder batch	Incrementally Solidified
6		3 mm
7		
8		
9		
10		
11		

Figure 7.
An experimental
stepwise LMH–AM
process of rod
construction in 11
repetitive steps

4. Modeling of localized microwave-heating for additive manufacturing

The temperature-dependent dielectric properties of iron powder (with no additives) were modeled as a cluster of iron spheres organized in a face-centered cubic (FCC) lattice, as illustrated in Figure 10. The iron spheres (20-μm diameter each) are isolated by their thin oxidation layer, represented in the simulation by air gaps (Ignatenko and Tanaka, 2010). Their macroscopic dielectric parameters were found by the method of *effective medium* approximation (Galek *et al.*, 2010). The simulated medium is arranged as an infinite FCC lattice in two dimensions, with two microwave ports defined in the third dimension. The scattering parameters simulated by COMSOL MultiPhysics[R] (Ver. 4.4) are used to extract the complex dielectric permittivity $\varepsilon(T)$ and magnetic permeability $\mu(T)$, which depend on both temperature and frequency (Jerby *et al.*, 2015). The magnetic losses are also attributed to the induced eddy currents (Galek *et al.*, 2010). As shown in the CST simulation in Figure 11(a) and (b), the current not only flows on the surface but also penetrates into the particle, owing to its finite electric conductivity σ of the metal. The resulted complex values of the effective magnetic permeability, $\mu_r(T) = \mu_r^{'}(T) - j\mu_r^{''}(T)$, are shown in Figure 12.

The simulated powder parameters listed in Table I are used for the macroscopic LMH model (Jerby *et al.*, 2015; Jerby *et al.*, 2005). The LMH interaction is mainly governed in this case by the magnetic component of the microwave radiation, as follows:
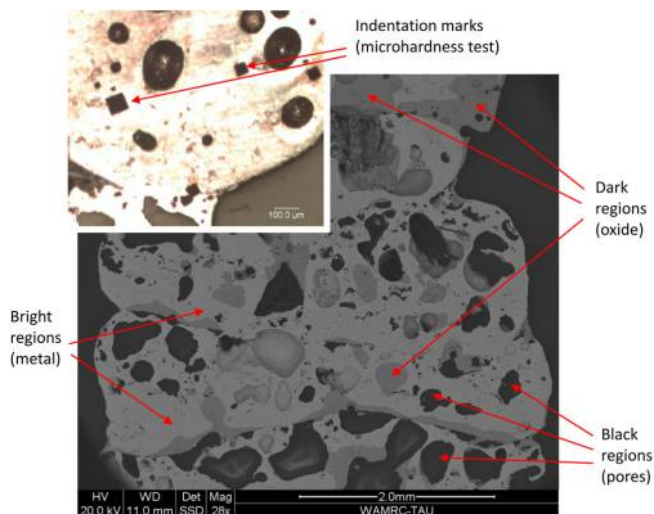
Note: The micrograph in the inset also shows the indentation
marks made by the microhardness tests with 0.5 and 1 kg loads, at
the metal and oxide regions

Figure 9.
A scanning electron
microscope (SEM)
BSE image of the
LMH product
microstructure,
revealing domains of
uniformly solidified
metal, oxide and
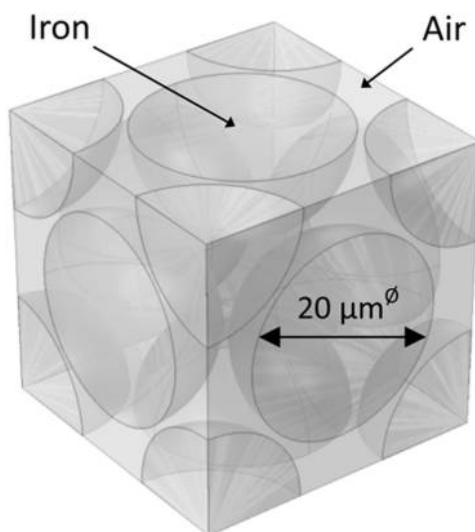pores (bright, dark
and black regions,
respectively)

Figure 10.
A powder model of
the periodic face-
centered cubic (FCC)
lattice of isolated iron
spheres used in the
numerical analyses

$$\nabla \times \nabla \times \widetilde{\mathbf{H}} - \mu_r(T)\varepsilon_r(T)k_0^2\widetilde{\mathbf{H}} = 0 \tag{3}$$

$$\rho c_p \partial T/\partial t - \nabla \cdot (k_{th}\nabla T) = Q \tag{4}$$

$$Q = \pi f\left(\mu_0 \mu_r^{''}|\widetilde{\mathbf{H}}|^2 + \varepsilon_0 \varepsilon_r^{''}|\widetilde{\mathbf{E}}|^2\right) \tag{5}$$

Figure 11.
(a) The current density evolved in the powder particle during LMH, simulated by CST, and (b) the eddy current density on the surface (in red) is more than ×10 denser than in the core (in blue)
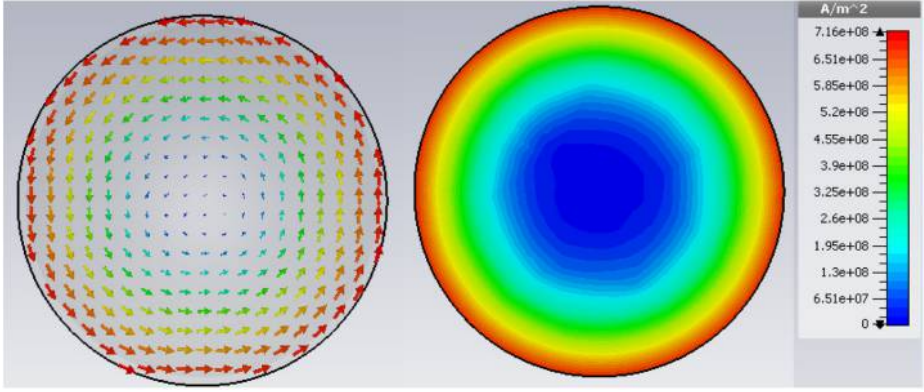
Figure 12.
The effective real and imaginary components of the relative magnetic permeability, $\mu_{r}(T) = \mu_r'(T) - j\mu_r^{''}(T)$, resulted from the particle simulation

Parameter	Symbol	Numerical value
Relative dielectric permittivity	ε_r	7.965
Relative magnetic permeability	$\mu_r(T)$	Complex variables shown in Figure 12
Heat capacity	c_P	390-430 J/kgK @ 290-890 K (linearly)
Thermal conductivity	k_{th}	0.0675-0.1575 W/mK @ 290-890 K (linearly)
Mass density	ρ	5,037 kg/m³
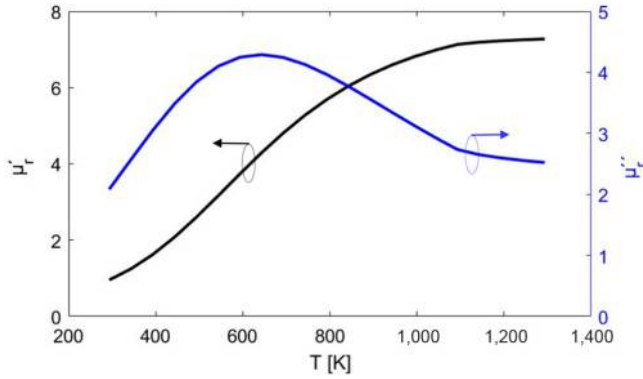
Table I.
Powder's effective parameters used for the LMH simulation

where $\widetilde{H}$ and $\widetilde{E}$ are the magnetic and electric field components, respectively, of the linearly polarized EM-wave at the operating frequency f and k_0 is its wavenumber in vacuum at this frequency. The metal powder is characterized by ρ, c_p and k_{th}, namely, its effective density, heat capacity and thermal conductivity, respectively. Equations (3 and 4), coupled by the dissipated power Q (5) and by the temperature profile, are solved by finite elements to simulate the temporal and spatial evolution of the hotspot temperature profile within the powder batch.

Figure 13 presents the simulated evolution of the temperature profile within the magnetically confined powder-batch. The absorbed (effective) microwave power in the simulation has been reduced to 40 W and less, to fit the measured temperature increase rate in Figure 6. This result means that most of the incident microwave power in this experiment is not absorbed by the powder batch but rather by a parasite load, most likely the plasma plume. Another possible effect associated with the plasma is the flash sintering mechanism (Bykov *et al.*, 2016) which could be significant in this process. Ignoring these plasma effects in the simulation, at the beginning of the heating process [Figure 13(a)], the temperature rises on the surface closer to the microwave source; then it evolves on the outer surface around [Figure 13(b)] and finally it penetrates into the powder batch in a more uniform heating pattern [Figure 13(c)]. According to these simulation results, the powder batch starts to melt from its bottom [Figure 13(a)] unlike the experimental observations, in which the higher temperature is seen first on the top of the batch. This discrepancy may also be attributed to the ejected plasma, which is not included in this simulation.

5. Discussion
This study confirms the feasibility of the incremental solidification process of magnetically confined metal powder-batches by LMH, as proposed in Jerby *et al.* (2015). The experimental results demonstrate the contact-less LMH–AM technique, and both simulation and experiment show that the magnetic confinement of the metal-powder batch enables its fixation. No mechanical support is needed during the microwave irradiation periods; hence, the LMH–AM process is significantly simplified.
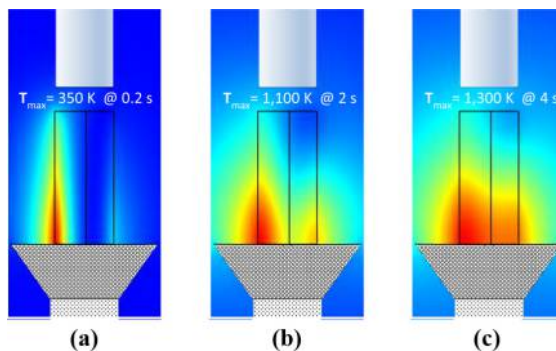
Notes: The temperature profile evolved is shown at (a) $t = 0.2$ s; (b) $t = 2$ s; (c) $t = 4$ s with the maximal temperature attained

Figure 13.
A simulation of the hotspot evolved by LMH within the powder-batch, between the lower movable stage and the upper electrode, in the scheme shown in Figure 3(b), at a reduced power of 17 W

The size of the elementary voxel (and hence the LMH–AM resolution) achieved in these experiments is in the order of approximately 2-4 mm$^{\varnothing}$ diameter and approximately 1-2 mm height. These results represent a precision level which is significantly inferior with respect to the laser-based AM systems. It is concluded therefore that LMH in this scheme could only be suitable in relatively rough construction operations of large-volume products.

Despite the advantages of the non-contact operation [as compared to our previous LMH–AM study with encapsulated powder-batches (Jerby *et al.*, 2015)], the drawbacks encountered in this experimental scheme are:

- The more intense plasma emission during the LMH process, which significantly reduces its efficiency; and
- The higher levels of oxidation and porosity of the product obtained.

Future experiments will be oriented, therefore, to overcoming these flaws by conducting the LMH–AM interaction in an inert gas atmosphere, as well as with denser powder-batches and lower microwave power (Shelef *et al.*, 2017).

The LMH–AM technique exhibits the selectivity feature of the microwave energy between the powder and bulk materials. Thus, it is expected that the resolution could be improved by using smaller amounts of powder in each batch, and a more precise placement of the powder-batch. Shorter microwave wavelengths at higher operating frequencies (e.g. millimeter waves) may also increase the voxel resolution. Preheating the powder shall also improve its initial coupling with the microwave energy, hence expedite the LMH process.

In addition to the powder confinement studied here, magnetic fields may also be used to manipulate the powder (Vandewalle and Lumay, 2009). In particular, the powder flow can be modulated by a variable magnetic field (as a contact-less valve) and even be divided to batches. This phenomenon can be used in future systems to regulate the powder flow during a continuous LMH–AM process (note that the relatively weak magnetic field required here can be easily generated and switched on and off by electromagnets). A continuous operating mode in an oxygen-free atmosphere (such as in TIG welding) may also improve the mechanical properties of the LMH–AM product.

These conclusions lead to a further study of LMH–AM in an inert-gas environment, which eliminates the plasma ejection and hence reduces the microwave power required to a level of approximately 100 W or less. This power reduction enables the combination of a compact solid-state microwave applicator [e.g. an LDMOS LMH device (Meir and Jerby, 2012)] with the magnetic-confinement mechanism of the powder in an integrated LMH–AM process. A more recent experiment in this approach have yielded preliminary results (Shelef *et al.*, 2017) encouraging further research and development of compact, low-cost devices for LMH–AM operations.

References

Bykov, Y.V., Egorov, S.V., Eremeev, A.G., Kholoptsev, V.V., Plotnikov, I.V., Rybakov, K.I. and Sorokin, A.A. (2016), "On the mechanism of microwave flash sintering of ceramics", *Materials*, Vol. 9 No. 8, Art. No. 684.

Conne, B.P., Manogharan, G.P., Martof, A.N., Rodomsky, L.M., Rodomsky, C.M., Jordan, D.C. and Limperos, J.W. (2014), "Making sense of 3-D printing: creating a map of additive manufacturing products and services", *Additive Manufacturing*, Vols 1/4, pp. 64-76.

Frazier, W.E. (2014), "Metal additive manufacturing: a review", *Journal of Materials Engineering and Performance*, Vol. 23 No. 6, pp. 1917-1928.

Galek, T., Porath, K., Burkel, E. and van Rienen, U. (2010), "Extraction of effective permittivity and permeability of metallic powders in the microwave range", *Modelling and Simulation in Materials Science and Engineering*, Vol. 18 No. 2, pp. 1-3. Art. No. 025015.

Griffiths, D.J. (2007), *Introduction to Electrodynamics*, 3rd Edition, Prentice Hall, New York, NY.

Herminghaus, S. (2005), "Dynamics of wet granular matter", *Advances in Physics*, Vol. 54 No. 3, pp. 221-261.

Ignatenko, M. and Tanaka, M. (2010), "Effective permittivity and permeability of coated metal powders at microwave frequency", *Physica B*, Vol. 405 No. 1, pp. 352-358.

Jerby, E., Aktushev, O. and Dikhtyar, V. (2005), "Theoretical analysis of the microwave-drill near-field localized heating effect", *Journal of Applied Physics*, Vol. 97 No. 3, Art. No. 034909.

Jerby, E., Dikhtyar, V., Aktushev, O. and Grosglick, U. (2002), "The microwave drill", *Science (New York, NY)*, Vol. 298 No. 5593, pp. 587-589.

Jerby, E., Meir, Y., Salzberg, A., Aharoni, E., Levy, A., Planta Torralba, J. and Cavallin, B. (2015), "Incremental metal-powder solidification by localized microwave-heating and its potential for additive manufacturing", *Additive Manufacturing*, Vol. 6, pp. 53-66.

Levy, G.N., Schindel, R. and Kruth, J.P. (2003), "Rapid manufacturing and rapid tooling with layer manufacturing (LM) technologies, state of the art and future perspectives", *CIRP Annals Manufacturing Technology*, Vol. 52 No. 2, pp. 589-609.

Li, C.H., Fang, Z. and Zhao, H.Y. (2010), "Investigation into layered manufacturing technologies for industrial applications", *2nd International Conference on Multimedia & Information Technology*, *Kaifeng*, pp. 213-216.

Lumay, G., Dorbolo, S. and Vandewalle, N. (2009), "Compaction dynamics of a magnetized powder", *Physical Review. E, Statistical, Nonlinear, and Soft Matter Physics*, Vol. 80 No. 4 Pt 1, p. 041302.

Meir, Y. and Jerby, E. (2012), "Localized rapid heating by low-power solid-state microwave-drill", *IEEE Transactions on Microwave Theory and Techniques*, Vol. 60 No. 8, pp. 2665-2672.

Mishra, R.R. and Sharma, A.K. (2016), "A review of research trends in microwave processing of metal-based materials and opportunities in microwave metal casting", *Critical Reviews in Solid-State and Materials Sciences*, Vol. 41 No. 3, pp. 217-255.

Roy, R., Agrawal, D. and Cheng, J. (1999), "Full sintering of powdered-metal bodies in a microwave field", *Nature*, Vol. 399 No. 6737, pp. 668-670.

Santos, E., Shiomi, M., Osakada, K. and Laoui, T. (2006), "Rapid manufacturing of metal components by laser forming", *International Journal of Machine Tools and Manufacture*, Vol. 46 Nos 12/13, pp. 1459-1468.

Shelef, A., Nerovni, Y., Fugenfirov, M. and Jerby, E. (2017), "Towards 3D-printing and additive manufacturing by localized microwave-heating of metal powders", *16th International Conference on Microwave and High-Frequency Heating, AMPERE-2017, Delft*, (18-21 September).

Sih, S. S. and Barlow, J.W. (2004), "The prediction of the emissivity and thermal conductivity of powder beds", *Particulate Science & Technology*, Vol. 22, pp. 291-304.

Vandewalle, N. and Lumay, G. (2009), "Flow properties and heap shape of magnetic powders", *AIP Conference Proceedings*, Vol. 1145 No. 135.

Wang, M., He, L. and Yin, Y. (2013), "Magnetic field guided colloidal assembly", *Materials Today*, Vol. 16 No. 4, pp. 110-116.

Corresponding author

Eli Jerby can be contacted at: jerby@eng.tau.ac.il